Aerodynamic and Aeroacoustic Performance of Spanwise Morphed Airfoils

Hasan Kamliya Jawahar*, Bin Zang†,
and
Mahdi Azarpeyvand‡
University of Bristol, Bristol, United Kingdom, BS8 1TR

Experimental studies of a NACA 0012 airfoil fitted with six different spanwise morphed flap profiles were successfully carried out to characterize their aerodynamic and aeroacoustic performance. The airfoil was tested with six configurations with different spanwise flap camber with a maximum deflection angle of $\beta = 10^\circ$ on one side and a minimum deflection angle of $\beta = 0^\circ$ on the other side. The tests were carried out for a flow velocity of $U_\infty = 20$ m/s, corresponding to a chord-based $Re_c = 2.6 \times 10^5$. The aerodynamic lift and drag measurements showed that improved lift-to-drag performance is highly dependant on the spanwise flap camber. Flow measurements at the downstream wake locations were carried out using hot-wire anemometry. Flow measurements also showed that the downstream wake development could be significantly influenced by the spanwise flap profile. The turbulent kinetic energy results displayed a characteristic double peak behavior at some locations along the span of the airfoil flap. Some of the tested cases had larger regions of double peak behavior along the span compared to the others. Aeroacoustic measurements were carried out using a beamforming array placed at a distance of 1 m. The beamforming map showed that the noise levels along the span are highly dependant on the spanwise camber of the morphed trailing edge and they portray possible noise reduction at select frequencies.

Nomenclature

b	=	trailing-edge flap length, m
c	=	airfoil chord length, m
C_L	=	lift coefficient
C_D	=	drag coefficient
l	=	airfoil span length, m
l_s	=	spanwise morphed trailing-edge length, m
k	=	turbulent kinetic energy, m^2/s^2
M	=	Mach number
p_{ref}	=	reference pressure ($= 2 \times 10^{-5}$), Pa
Re_c	=	chord-based Reynolds number
U_∞	=	free-stream velocity, m/s
U	=	mean streamwise velocity, m/s
V	=	mean crosswise velocity, m/s
τ	=	Reynolds shear stress component
x, y, z	=	streamwise, crosswise and spanwise coordinates, m
α	=	angle of attack, °
β	=	morphing flap tip deflection angle, °

*Corresponding Author, Research Associate, Department of Aerospace Engineering, hasan.kj@bristol.ac.uk
†Research Associate, Department of Aerospace Engineering, nick.zang@bristol.ac.uk
‡Professor in Aeroacoustics, Department of Mechanical Engineering, m.azarpeyvand@bristol.ac.uk

I. Introduction

THE advent of shape-adaptive structures in recent times has led to improved aerodynamic performance of wind turbine blades and airplane wings by reducing its weight and complexity. These structures contain smooth geometric changes and continuous structural surfaces while remaining conformal to the flow and are often referred to as morphing structures. The use of morphing structures is expected to give significant noise and drag reduction. It is very important in the design concept of morphing structures to thoroughly investigate the flow behaviors and mechanisms of performance improvement.

Studies have shown that noise generated by kinetic energy scattering of turbulent eddies in the boundary layer become dominant as they pass over the airfoil trailing-edge [1]. As such, airfoil self-noise has been considered as an important component of airframe noise during take-off and landing. Some of the currently employed passive methods for airfoil trailing-edge noise reduction includes serrated trailing-edges [3–7], porous surface treatments [8–10] and morphing structures [11–17]. With the use of morphing surfaces, we aim to address transition delay, separation postponement, lift enhancement, drag reduction, turbulence augmentation, and noise suppression [25]. An ideal method of morphing should achieve the control goal without affecting other goals, adversely. However, in reality, continuous compromises and trade-offs have to be made for a particular design goal as it is almost impossible to decouple the interlinked flow behavior [25], i.e. lift and drag forces and noise emission in the case of the high-lift systems.

Several studies of morphing structures have shown that smooth curvature has significant effects on the aerodynamic performance of airfoils. Most studies focused on the morphing structures and mechanism [26–32] rather than the aerodynamic and aeroacoustic performance of morphing airfoils. An innovative trailing-edge morphing mechanism that uses a honeycomb core with axial variable stiffness developed by Ai *et al.* [31, 32], was used as morphing profile for the experimental and computational studies carried out by Jawahar *et al.* [14–17]. The recent study by Jawahar *et al.* [17] showed that small changes in the flap camber profile of the morphed flap can change the aerodynamic behavior significantly. The lift and drag were affected for flap with higher camber, producing larger lift as well as higher drag. The boundary layer behavior showed delayed separation for the morphed flap airfoil relative to the conventional hinged flap configuration. The turbulence levels at the wake were also found to be significantly altered with the morphed flap having a higher magnitude. This study concluded that independent surface morphing would aid the favorable delayed separation while reducing the unfavorable increased drag.

The flap side-edge noise is often identified as the dominant noise source from the flap [18]. The flap noise is a result of the vortical structures that arises due to the recirculation flow from the pressure jump across the upper and lower surfaces of the flap [19, 20]. The flap noise dominates the middle-to-high frequency range. Potential acoustic sources of a flap are vortex related and occur at the flap side edges. Therefore the flap noise reduction could be achieved by the use of side-edge treatments. Successful side edge treatments include side edge fences [20], porous flap edge [21] and edge brushes [22]. These treatments have demonstrated a significant reduction in radiated noise by weakening and elimination of the side edge vortices. Another approach is Continuous Mold-line Link flap where the side edge is eliminated by the use of a continuous mold-line link (CML) [23]. This works by splitting the single vortex at the edge into many small weaker vortices. Noise reduction of up to 10 dB in comparison with normal flaps can be achieved using this method. Pankonien and Iman [24] showed spanwise morphing trailing-edge improved relative aerodynamic performance by decreasing the relative effect of the inboard flap vortex with suggestions for further investigations on the subject. Therefore the paper aims to further our understanding of the aerodynamic and aeroacoustic benefits of various spanwise morphed trailing-edge. Complementing the authors' previous studies [14–17] the current experimental study investigates aerodynamic and aeroacoustic behavior of a spanwise morphed trailing-edge with a trip. This paper presents a detailed aerodynamic study with lift and drag measurements and wake flow field from hot-wire measurements, unsteady surface pressure fluctuations, and far-field measurements from beamforming array.

II. Experimental and wind tunnel setup

1. *Airfoil setup*

NACA 0012 airfoil fitted with six different spanwise morphed trailing-edge were experimentally tested at the University of Bristol. The tests were carried out at a freestream velocity of $U_\infty = 20$ m/s corresponding to a chord-based Reynolds number of $Re_c = 2.6 \times 10^5$ at Mach number $M \approx 0.058$. The tested NACA 0012 airfoil has a chord length of $c = 0.2$ m and a span length of $l = 0.45$ m. The airfoil was designed such that it facilitates the installation of two interchangeable trailing-edge flaps with a length of $b = 0.06$ m ($0.3c$). The airfoil was tested with a spanwise morphed trailing-edge as shown in Fig. 1. The airfoil's trailing-edge section comprises of three spanwise sections with a span of $l_s = 0.75c$ each: left section a chordwise morphed trailing-edge with a deflection angle of $\beta = 10°$, a right section

having the baseline line trailing-edge with a deflection angle of $\beta = 0°$ and a center spanwise morphed trailing-edge (SPM) section, a continuous morphing angle transition connecting the left and right section. In order to achieve a turbulent boundary layer over the trailing-edge and to prevent shear layer instabilities such as Tollmien-Schlichting waves from interfering with the noise measurements, the boundary layer was tripped at $0.1c$ on both sides of the airfoil with a serrated turbulator tape having a height of 0.5 mm and a serration angle of 60° [34, 35].

$$w(x) = \varphi(x)\beta,$$
$$\varphi(x) = \begin{cases} 0, & 0 \le x < c - b \\ \frac{(c-x-b)^3}{b^2}, & c - b \le x < c \end{cases} \tag{1}$$

In order to thoroughly examine the performance and mechanism of trailing-edge noise reduction with differently configured SPM, a total of a total of six SPM cases were tested (see Fig. 2). SPM-Case 3 represents an SPM trailing-edge shape with a constant slope between $\beta = 0°$ and 10° along the span. SPM-Case 1 and 5 have the highest spanwise slope resulting in a reduced area of the deflected trailing-edge for SPM-Case 1 and increased area of the deflected trailing-edge for SPM-Case 5. The slope of SPM-Case 2 and 3 is moderate as it lies between the constant slope Case 3 and extreme slope Cases 1 and 5, respectively. A benchmark case, labeled as SPM-Baseline and represented by the black dashed line in Fig. 2, is also proposed and studied which features a discontinuity of morphing angle transition at the mid-span position. For the trailing-edge design, it is assumed that the chordwise deformed profile of the SPMs and the morphing trailing-edge follow the polynomial deformation expressed in Eq. 1 [27], where c is the airfoil chord length and b is the morphing TE length. The five designed SPM cases were manufactured with rapid prototyping techniques.

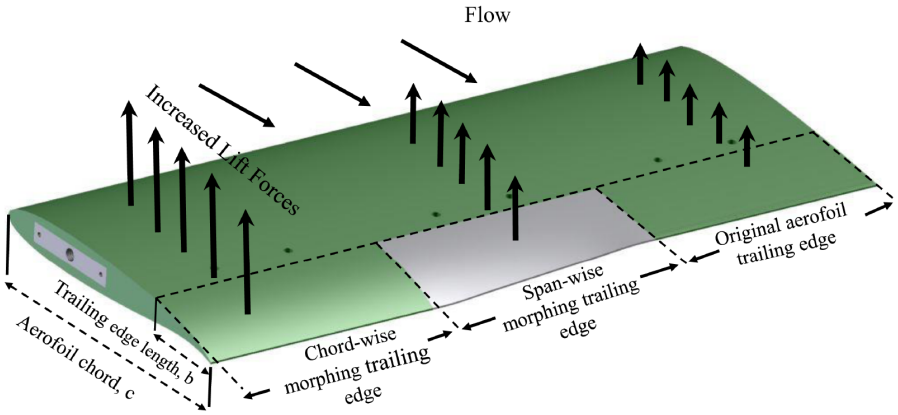

Fig. 1. Schematic of the NACA 0012 airfoil fitted with a chordwise and spanwise morphed trailing-edge.

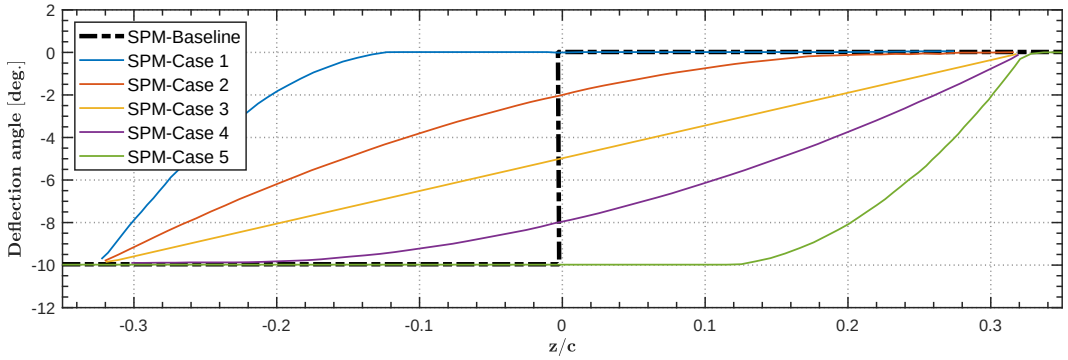

Fig. 2. Spanwise trailing-edge profiles of the various tested SPM configurations.

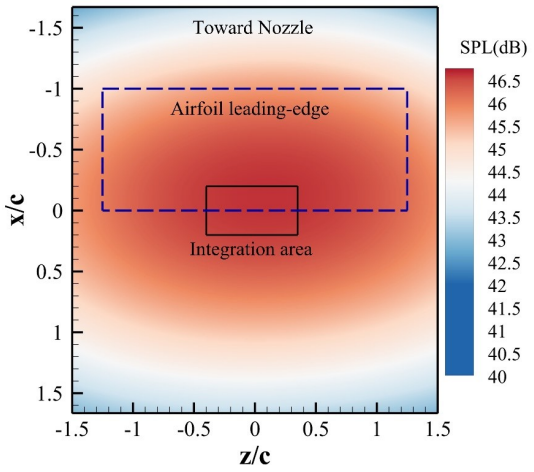

Fig. 3. Schematic of the beamforming contour map and its integration area used to determine the far-field noise spectra, at the central frequency of 1122 Hz for angle of attack $\alpha = 8°$

2. *Force measurement setup*

Aerodynamic measurements such as lift and drag were carried out at the University of Bristol open-jet wind tunnel with a circular test section diameter of 1.1 m, with a maximum reliable speed of 30 m/s and minimum turbulence level of 0.05%. The blockage effects were found to be negligible. The three-dimensionality effects of the flow around the airfoil model in the wind tunnel were mitigated with two circular end-plates with a radius of 0.17 m. The lift and drag forces of the various airfoil configurations were measured using an AMTI OR6-7-2000 force platform from Advanced Mechanical Technology Inc., mounted at the base of the set-up. The data were sampled at a frequency of 2000 Hz for a sampling period of 16 s for all the tests, these values were selected after a thorough uncertainty analysis of the results. The measurements were made for angles of attack $\alpha = -5°$ to $15°$ with an increment of $\alpha = 1°$ for all the SPM configurations.

3. *Wake measurements setup*

Steady and unsteady flow velocities were measured for a spanwise plane very close to the airfoil trailing-edge at a streamwise location $x/c = 0.05$ within the airfoil wake for all the six configurations at the University of Bristol Aeroacoustic wind tunnel [36]. The measurements were made using a Dantec 55P51 cross hot-wire probe with a 5 μm diameter and 1.25 mm long platinum-plated tungsten wire sensor for 850 points. The hot-wire and temperature probes were connected to the StreamWare Pro V5.14 software package, driven by Dantec Streamline Pro CTA 91C10 modules and controlled using National Instruments PXIe-4499 modules mounted in a National Instruments PXIe-1062Q chassis. Calibrations were conducted for the probe using a Dantec 54H10 two-point mode hot-wire calibrator. The data was logged at a frequency of 2^{15} Hz and a measurement duration of 8 seconds per point. The probe was mounted on a 1 m long slender cylindrical steel arm connected to the traverse system to minimize the bluff-body effects of the traverse system on the airfoil and wind tunnel. The measurements were made for angles of attack $\alpha = 0°$ and $8°$ for all the SPM configurations.

4. *Acoustic measurement setup*

Far-field noise measurements were carried out using a beamforming array placed at 1 m above the trailing-edge of the airfoil. The beamforming test section has 73 Panasonic WM-61A microphones equally distributed amongst 9 arms [37]. Figure 3 shows an example sound pressure level contour map determined from the beamforming array at a central frequency of 1122 Hz and the angle of attack, $\alpha = 8°$. Note that the SPL level was calculated using one-third octave band. As seen from the figure, the highest SPL level coincides quite well with that of the trailing-edge of the airfoil, suggesting that trailing-edge noise is indeed the primary noise source in the present experiments. To obtain the far-field noise spectra, a rectangular area having a length of $0.4c$ in streamwise and width of $0.75c$ in spanwise directions was spatially integrated covering the spanwise morphing trailing-edge area, where the SPL levels remain relatively constant with respect to the airfoil trailing-edge. Following the conventions, the final far-field noise spectra were subsequently corrected to correspond to the entire span of the airfoil [38].

III. Results and discussion

A. Aerodynamic Force Measurements

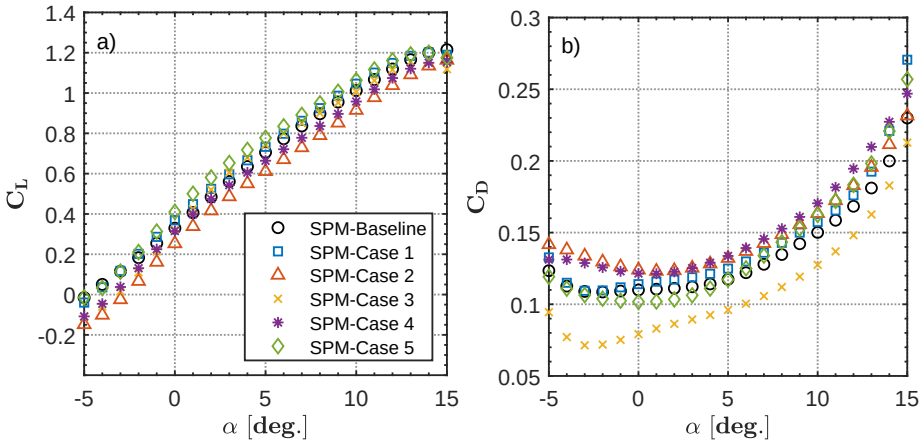

Fig. 4. Lift and drag coefficient results for all the SPM configurations at a freestream velocity of $U_\infty = 20$ m/s ($Re_c = 2.6 \times 10^5$).

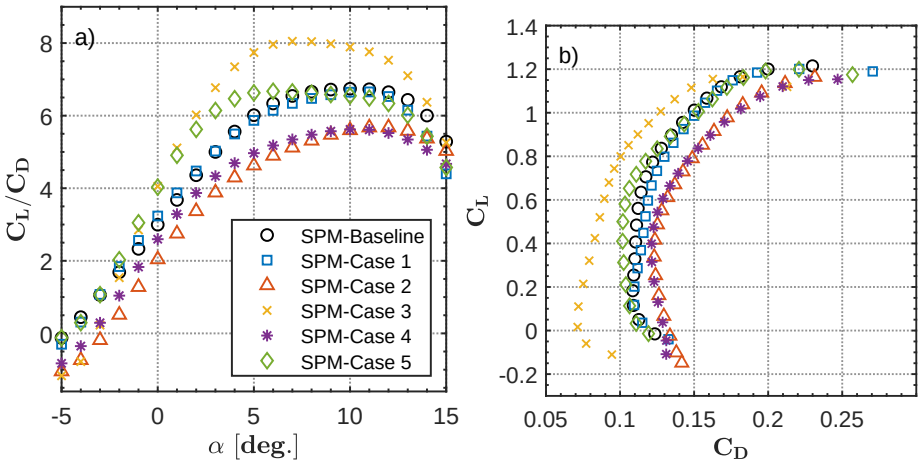

Fig. 5. Lift-to-drag coefficient ratio results and the drag polar plots for all the SPM configurations at a freestream velocity of $U_\infty = 20$ m/s ($Re_c = 2.6 \times 10^5$).

The results of the aerodynamic force measurements for NACA 0012 airfoil fitted with various SPM trailing-edge profiles are presented in Fig. 4. A serrated turbulator tape was used on both sides of the airfoil surface to make the boundary layer flow turbulent. The tests were carried out for angles of attack ranging from $\alpha = -5°$ to 15°. The results of the lift coefficients $C_L - \alpha$ presented in Fig. 4a show a better overall lift performance for SPM-Case 5 compared to the other configurations. The increased lift could be due to the larger area of the deflected trailing-edge for SPM-Case 5. The C_L-α curve of SPM-Case 2 has the lowest C_L compared to all the other SPM configurations over the tested angles of attack. The largest difference in the lift coefficient $\Delta C_L = 0.167$ amongst all the SPM configurations were produced at $\alpha = 4°$ between SPM-Case 2 and Case 5 and the ΔC_L between the cases started narrowing as the angle of attack was nearing stall. SPM-Case 5 with the highest C_L-α curve reduces the angle of attack for a given lift coefficient by 3° compared to SPM-Case 2, the case with the lowest C_L-α curve. The drag coefficient results $C_D - \alpha$ presented in Fig. 4b show a generic airfoil $C_D - \alpha$ trend with lower values of C_D at low angles of attack and increasing values of C_D as the angle of attack is increased. SPM-Case 3 results show the lowest levels of drag for the entire tested range of angles of attack compared to the other cases. The highest C_D between angles of attack $\alpha = -5 - 5$ and $\alpha = 5 - 15$ were found for SPM-Cases 2 and 4, respectively.

The lift-to-drag coefficient ratio results and the drag polar curves for all the SPM configurations are presented in Fig. 5. The results for the lift-to-drag coefficient ratio are presented in Fig. 5(a). The results show a large difference in the lift-to-drag coefficient ratio between tested SPM configurations at angles of attack between $\alpha = 5° - 12°$. SPM-

Case 3 has an overall superior aerodynamic lift performance compared to all the other SPM configurations at all the tested angles of attack. There is insignificant difference in the C_L/C_D performance between SPM-Case 2 and Case 4. However, compared to SPM-Case 1 and Case 5, SPM-Case 5 has superior aerodynamic behavior between angles of attack $\alpha = 0^\circ - 6^\circ$. The largest difference in the lift-to-drag coefficient ratio of $\Delta(C_L/C_D) = 2.93$ was found between SPM-Case 2 and Case 3 at the angle of attack $\alpha = 7^\circ$ with SPM-Case 3 portraying better performance with larger values of C_L/C_D. The largest value of $C_L/C_D = 8.05$ was achieved by SPM-Case 3 at $\alpha = 7^\circ$. The results for the drag polar curves are presented on the right side of the figure, in Fig.5(b). The result for SPM-Case 3 shows its superior aerodynamic performance with the lowest C_D for a given C_L compared to all the other cases. Overall the results show that for cases with the highest trailing-edge slop between SPM-Case 1 and 5, the latter shows better aerodynamic performance which could be attributed to the increased deflection area at the trailing-edge. Between SPM-Case 2 and 4, yet again the latter shows superior performance. The best aerodynamic performance was delivered by SPM-Case 3 over the entire range of tested angles of attack.

B. Wake flow analysis

Detailed flow field measurements at one downstream wake location on a spanwise plane were performed using hot-wire anemometry to further understand the flow behavior due to the spanwise camber profile at the trailing-edge. The wake measurements were carried out for NACA 0012 airfoil fitted with various SPM trailing-edge configuration. Only one downstream wake location $x/c = 0.05$ at the vicinity of the airfoil trailing-edge was selected for the wake development study. The tests were performed in the Aeroacoustic wind tunnel for angles of attack, $\alpha = 0^\circ$ and 8° at flow velocity $U_\infty = 20$ m/s, corresponding to $Re_c = 2.6 \times 10^5$. For the purpose of brevity, only the results of 8° are presented here.

The results of the non-dimensional streamwise velocity (U/U_∞), crosswise velocity (V/U_∞) and turbulent kinetic energy (TKE, k/U_∞) contours at angles of attack $\alpha = 8^\circ$ for all the various configurations are presented in Figs. 6 to 7. The results are presented in terms of spanwise location on the x-axis and crosswise location on the y-axis at the airfoil wake. The results are presented in three columns with the non-dimensional streamwise velocity, crosswise velocity, and TKE contours from left to right, respectively, and different cases are presented in different rows. The results for SPM-Baseline presented in Fig. 6 clearly show the discontinuity in the mid-span between $\beta = 0^\circ$ and 10°. The non-dimensional streamwise velocity for SPM-Baseline in Fig. 6(a) shows an increased velocity deficit for the left section with $\beta = 10^\circ$ relative to the section with $\beta = 0^\circ$ on the right. A similar trend with increased TKE for the left section of SPM-Baseline can be observed in Fig. 6(c). The results for the non-dimensional crosswise velocity show increased downward flow over the $\beta = 10^\circ$ on the left as expected. However, a prominent high V/U_∞ values and TKE can be observed in the mid-span region with the span discontinuity.

The wake flow field results for all of the tested SPM variants are presented in Fig. 7. The results for SPM cases with the extremely morphed cases with the highest slope, SPM-Case 1, and 5 show reduced streamwise velocity deficit at the slope transition location. The V/U_∞ shows a smaller area of downward flow deflection for SPM-Case 1 compared to Case 5, which also corresponds to the increased lift characteristics seen earlier for SPM-Case 5. SPM-Case 1 also shows reduced regions with high TKE compared to the Case 5, which might result in relatively reduced trailing-edge noise. The V/U_∞ results for SPM-Case 2 and 4 with moderately morphed trailing-edge, show that the case with profile deflection towards the lower surface (SPM-Case 4) has a larger area with downward flow deflection relative to SPM-Case 2 that might have aided in the increased aerodynamic performance seen earlier. However, SPM-Case 4 shows increased TKE along the span compared to SPM-Case 4. The aerodynamically superior SPM-Case 3 with constant morphed trailing-edge shows increased downward deflection over a larger area compared to SPM-Case 1, 2, and 4. The gradual change in the trailing-edge profile appears to be favorable for flow downwash and reduced TKE, which may have played a crucial role in modifying the behavior of the radiated far-field noise..

C. Acoustic analysis

To first establish the characteristics of the beamforming array and to examine the general behavior of the measured far-field noise, SPL contour maps determined from the beamforming array between the baseline and the spanwise morphed trailing-edge airfoils at different frequencies of interest are presented in Figs. 9 and 10. To begin with, Fig. 9 depicts the SPL contour maps at relatively low frequencies to reassure the validity of the beamforming array measurements. As seen in Fig. 9(a) for SPM-Baseline, the regions centered around the trailing-edge produce the highest SPL level and therefore recognized as the primary source of radiated noise. Moreover, the contour map is essentially symmetric about the center of the trailing-edge, $x/c = 0$, which should be expected in the baseline configuration. Nevertheless, when the baseline is replaced with the spanwise morphed trailing-edges, the symmetry ceases to exist, rather the contour becomes lopsided toward the positive spanwise direction, starting from approximately $x/c = 0.4$, for all the spanwise morphed trailing-edge cases. Such behavior points to a possible strong gap noise in the junction between the morphed structure and the airfoil, as it is present irrespective of the various morphing topologies. As a result, care has been taken when performing the spatial integration over the trailing-edge area at low frequencies, to only include areas with relatively constant SPL levels. The beamforming maps around the airfoil were first calculated and then the area around spanwise morphed trailing-edge was integrated to calculate the sound pressure level (SPL) as shown in Fig. 3. The results for the integrated SPL levels around the spanwise morphed trailing-edge for angles of attack $\alpha = 0°$ and $8°$ are presented in Fig.8. SPL results for $\alpha = 8°$ show similar results between all of the tested cases but some slight discrepancies at moderate to high frequencies such as 2500 Hz, 3150 Hz, and 4000 Hz.

Since the present study is more interested in the moderate to high frequencies, Fig. 10 shows the SPL contour maps for the baseline and spanwise morphed trailing-edge airfoils at 2500 Hz, 3150 Hz and 4000 Hz. Similar to the low-frequency scenario, the spanwise morphed trailing-edge show more accentuated asymmetry than that of the baseline configuration, however, the extent has been considerably diminished as the frequency increases. More importantly, the morphed trailing-edge can be observed to cause a notable reduction in the SPL and thus likely lead to a reduction in the radiated far-field noise. For instance, the maximum SPL levels for the baseline trailing-edge are 35, 33, and 32 for the frequencies of 2500 Hz, 3150 Hz and 4000 Hz, respectively, whereas, they are 33, 30 and 28 for SPM-Case 1 morphed trailing-edge. Therefore, the application of spanwise morphed trailing-edge appears to be effective in the reduction of the SPL levels from beamforming contour maps at relatively higher frequencies. SPM-Case 3 shows reduced noise levels around the spanwise morphed especially at 3150 Hz.

Relating the noise measurement results to the wake velocity energy contents, the contours of the wake spectra for the frequencies of interest (2500 Hz, 3150 Hz, and 4000 Hz) calculated from the hotwire streamwise velocity fluctuation are plotted in Figs. 12 and 11. The results for SPM-Baseline configuration in Fig.12 show relatively increased energy content at the mid-span region with the trailing edge discontinuity for all the presented frequencies, which is in direct constrast to the the morphed trailing-edge cases in Fig. 11. For SPM-Case 1 and 5 with the most extreme trailing edge slope, high energy content for the presented frequencies can be found at the highest slope region for both cases. For SPM-Case 2 and 4 with a moderate trailing edge slope, SPM-Case 4 shows larger area with higher energy content. The best performing SPM-Case 3 yet again shows relatively evenly distributed energy levels along the span compared to all the other tested cases.

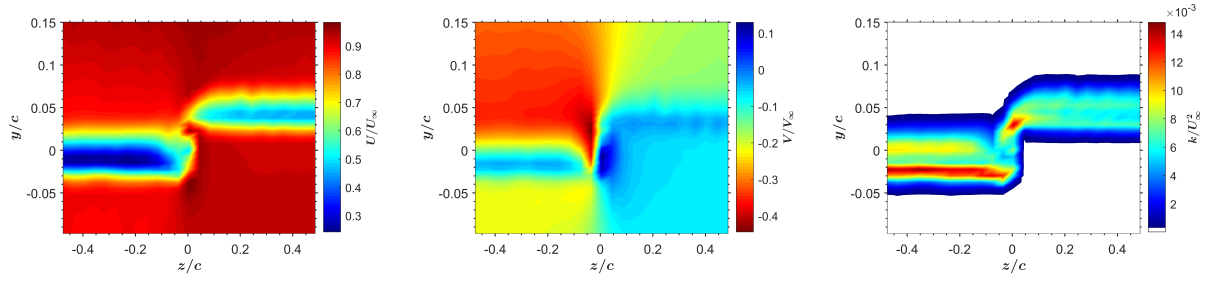

a) SPM-Baseline, U/U_∞ **b) SPM-Baseline, V/U_∞** **c) SPM-Baseline, k/U_∞^2**

Fig. 6. The non-dimensional streamwise velocity, crosswise velocity and turbulent kinetic energy contours for a spanwise plane at the wake location $x/c = 0.05$ for SPM-Baseline airfoil at the angle of attack $\alpha = 8°$.

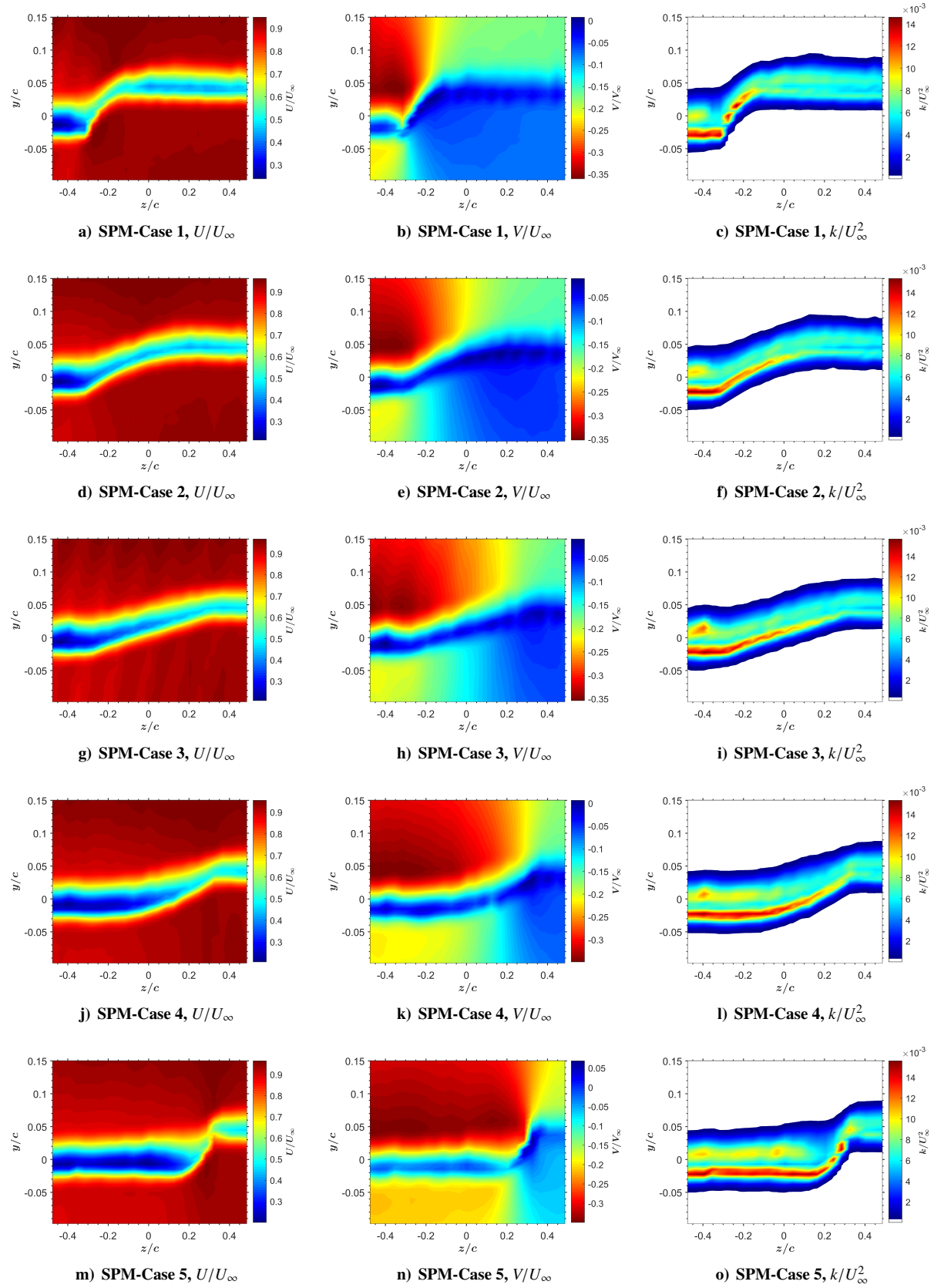

a) SPM-Case 1, U/U_∞ **b) SPM-Case 1,** V/U_∞ **c) SPM-Case 1,** k/U_∞^2

d) SPM-Case 2, U/U_∞ **e) SPM-Case 2,** V/U_∞ **f) SPM-Case 2,** k/U_∞^2

g) SPM-Case 3, U/U_∞ **h) SPM-Case 3,** V/U_∞ **i) SPM-Case 3,** k/U_∞^2

j) SPM-Case 4, U/U_∞ **k) SPM-Case 4,** V/U_∞ **l) SPM-Case 4,** k/U_∞^2

m) SPM-Case 5, U/U_∞ **n) SPM-Case 5,** V/U_∞ **o) SPM-Case 5,** k/U_∞^2

Fig. 7. The non-dimensional streamwise velocity, crosswise velocity and turbulent kinetic energy contours for a spanwise plane at the wake location $x/c = 0.05$ **for various SPM configurations (SPM-Case 1-5) at the angle of attack** $\alpha = 8°$**.**

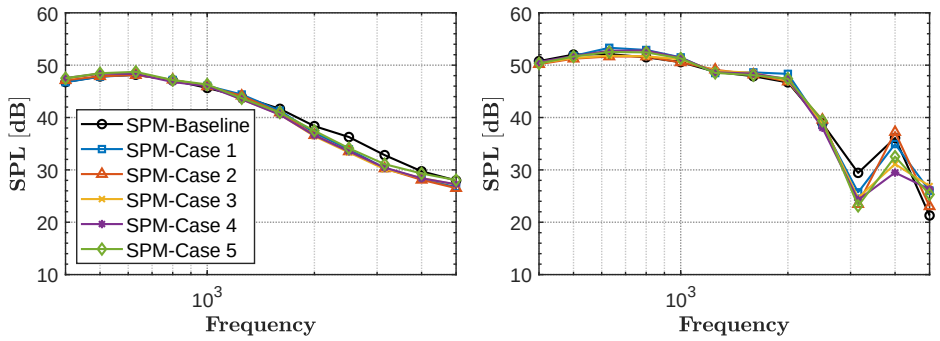

a) $\alpha = 0°$ **b)** $\alpha = 8°$

Fig. 8. Far-field noise intergrated around spanwise morphing-trailing edge from the beamforming measurements.

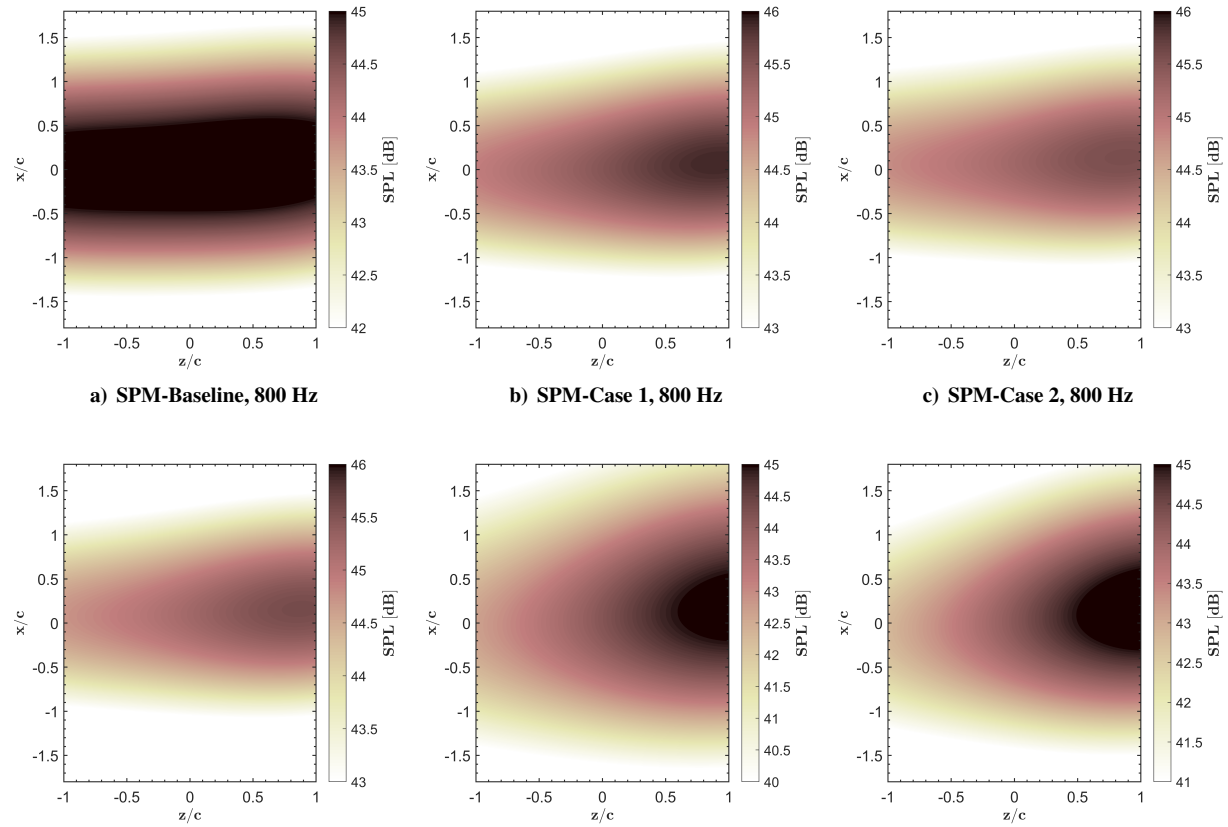

a) SPM-Baseline, 800 Hz **b) SPM-Case 1, 800 Hz** **c) SPM-Case 2, 800 Hz**

d) SPM-Case 3, 800 Hz **e) SPM-Case 4, 800 Hz** **f) SPM-Case 5, 800 Hz**

Fig. 9. Beamforming map at 800 Hz for various SPM configurations at the angle of attack $\alpha = 8°$.

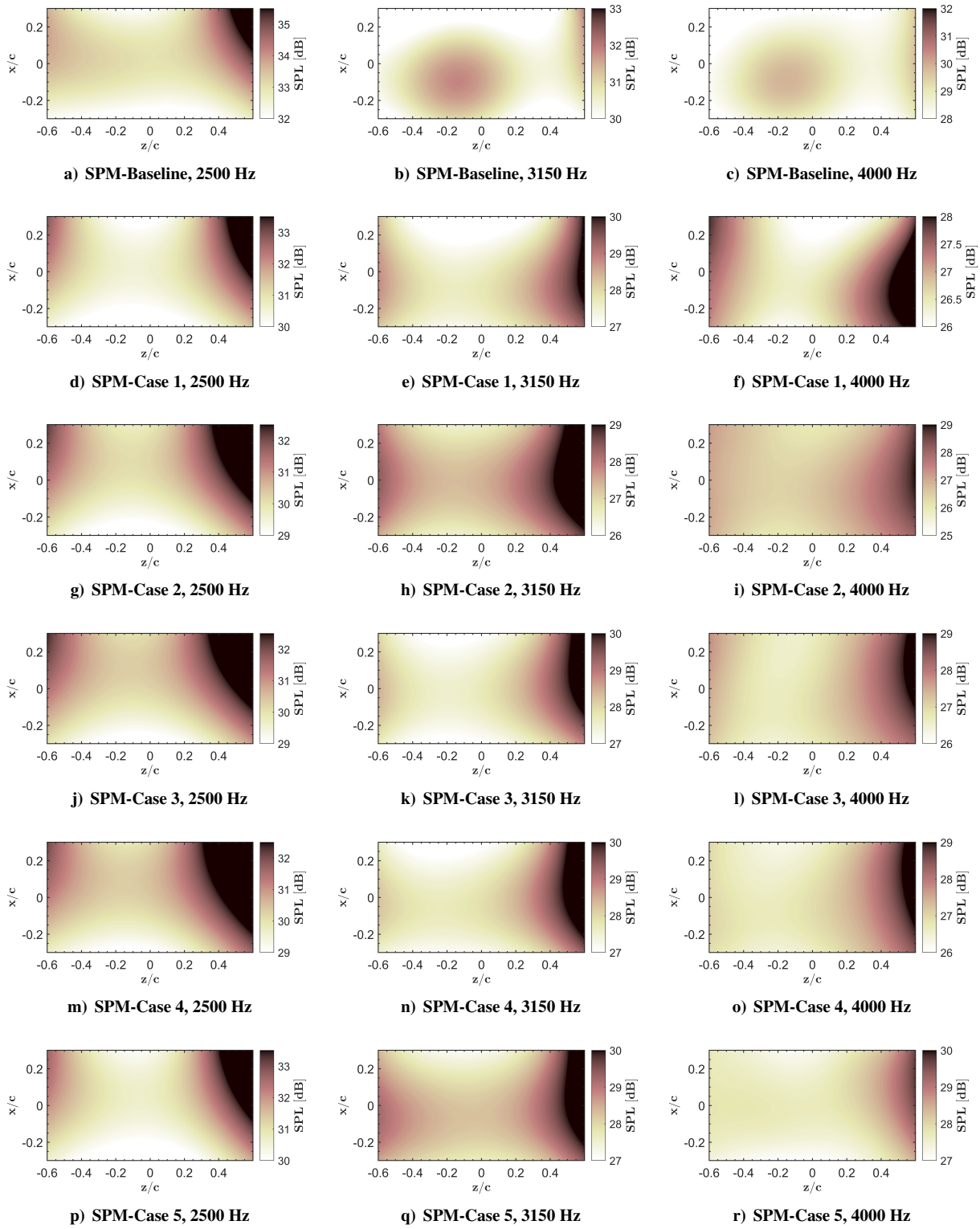

a) SPM-Baseline, 2500 Hz
b) SPM-Baseline, 3150 Hz
c) SPM-Baseline, 4000 Hz
d) SPM-Case 1, 2500 Hz
e) SPM-Case 1, 3150 Hz
f) SPM-Case 1, 4000 Hz
g) SPM-Case 2, 2500 Hz
h) SPM-Case 2, 3150 Hz
i) SPM-Case 2, 4000 Hz
j) SPM-Case 3, 2500 Hz
k) SPM-Case 3, 3150 Hz
l) SPM-Case 3, 4000 Hz
m) SPM-Case 4, 2500 Hz
n) SPM-Case 4, 3150 Hz
o) SPM-Case 4, 4000 Hz
p) SPM-Case 5, 2500 Hz
q) SPM-Case 5, 3150 Hz
r) SPM-Case 5, 4000 Hz

Fig. 10. Beamforming map at three frequencies of interest (2500, 3150 and 4000 Hz) for various SPM configurations at the angle of attack $\alpha = 8°$.

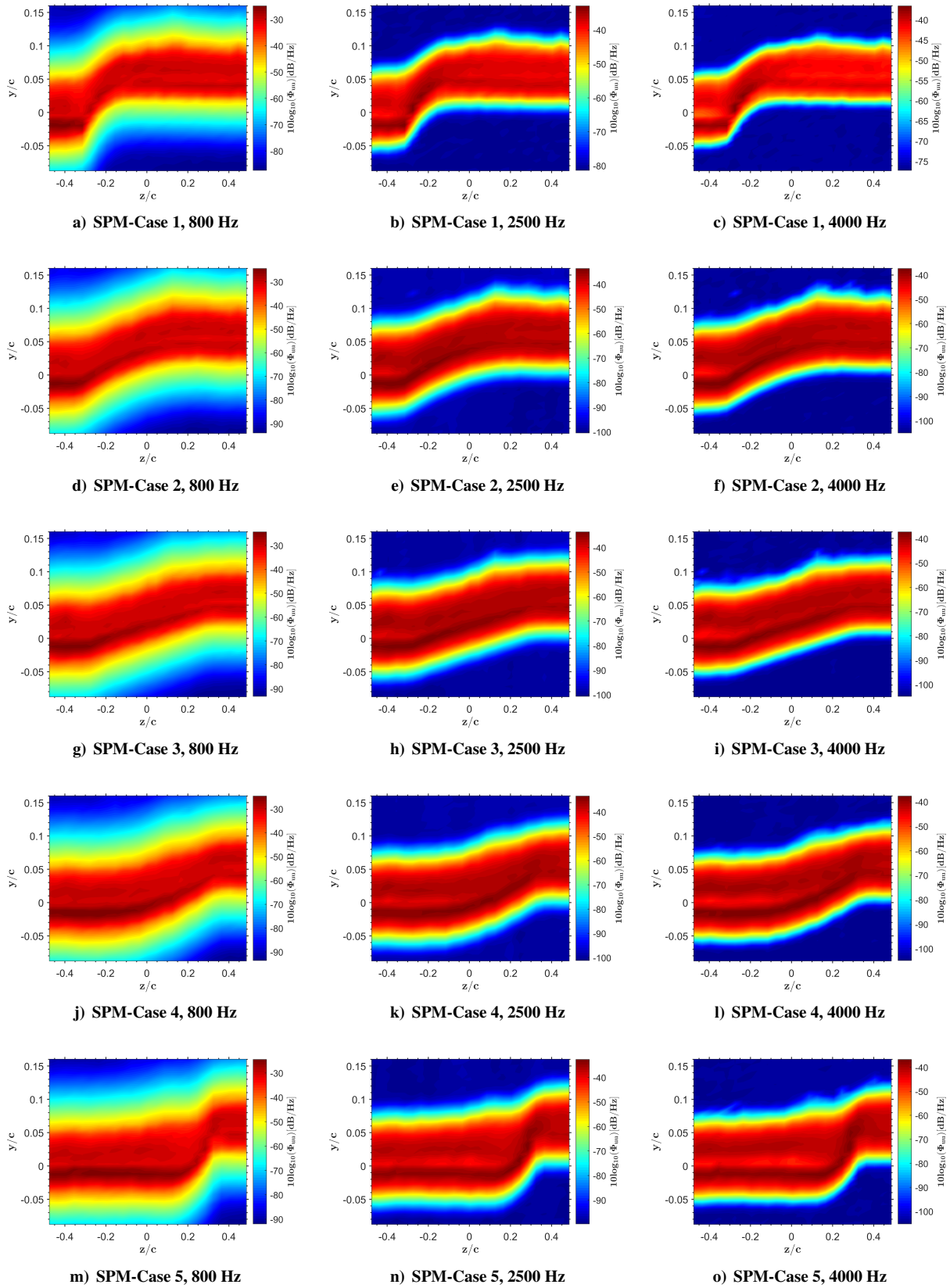

a) SPM-Case 1, 800 Hz | b) SPM-Case 1, 2500 Hz | c) SPM-Case 1, 4000 Hz

d) SPM-Case 2, 800 Hz | e) SPM-Case 2, 2500 Hz | f) SPM-Case 2, 4000 Hz

g) SPM-Case 3, 800 Hz | h) SPM-Case 3, 2500 Hz | i) SPM-Case 3, 4000 Hz

j) SPM-Case 4, 800 Hz | k) SPM-Case 4, 2500 Hz | l) SPM-Case 4, 4000 Hz

m) SPM-Case 5, 800 Hz | n) SPM-Case 5, 2500 Hz | o) SPM-Case 5, 4000 Hz

Fig. 11. The non-dimensional streamwise velocity fluctuations for a spanwise plane at the wake location $x/c = 0.05$ for various SPM configurations (SPM-Case 1-5) at the angle of attack $\alpha = 8°$.

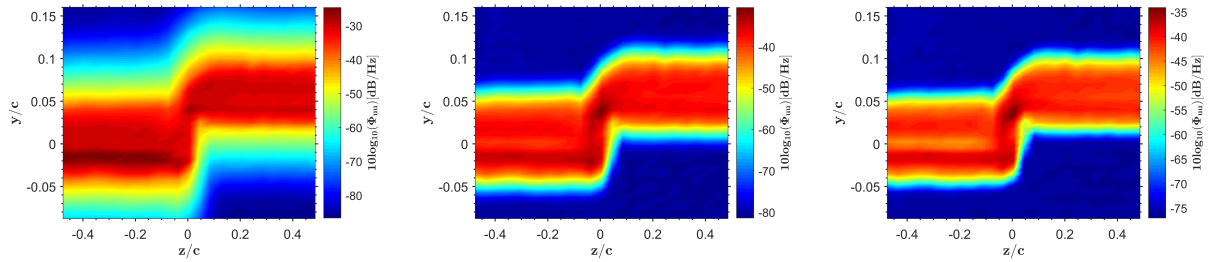

a) SPM-Baseline, 800 Hz **b) SPM-Baseline, 2500 Hz** **c) SPM-Baseline, 3150 Hz**

Fig. 12. The non-dimensional streamwise velocity fluctuations for a spanwise plane at the wake location $x/c = 0.05$ for SPM-Baseline airfoil at the angle of attack $\alpha = 0°$.

IV. Conclusion

The aerodynamic and aeroacoustic performance of NACA 0012 airfoil fitted with six different spanwise morphed trailing-edge were investigated using experimental techniques. The airfoil was tested for a flow velocity of U_∞ = 20 m/s, corresponding to a chord-based $Re_c = 2.6 \times 10^5$. Aerodynamic lift and drag measurements and flow measurements using hot-wire anemometry were carried out to better understand the flow characteristics of the spanwise morphed trailing-edges. The lift and drag measurements showed that the spanwise morphed trailing-edge profile has a substantial effect on the aerodynamic behavior of the airfoil and the best overall aerodynamic performance was portrayed by SPM-Case 3 compared to all the tested SPM configurations. The wake flow field results also showed a large area of downward flow deflection and distributed TKE for SPM-Case 3. The acoustic measurements were carried out using beamforming array and the results are evident that spanwise morphing leads to noise reduction for certain frequencies. The wake energy spectra showed that reduction in noise for certain frequencies is due to the severity in the change in the shape of the trailing edge therefore relatively better performance was observed for SPM-Case 3.

References

[1] Lockard, D.P., and Lilley, G.M., *The Airframe Noise Reduction Challenge*, NASA-TM-2004-213013, 2004.

[2] Wagner, S., Bareriss, R., and Guidati, G. *Wind Turbine Noise*, Springer: Berlin, 1996, pp: 67-92.

[3] Liu, X., Kamliya Jawahar, H., Azarpeyvand, M., and Theunissen, R. "Aerodynamic Performance and Wake Development of Airfoils with Serrated trailing-edges", AIAA Journal, Vol. 55, No. 11 (2017), pp: 3669-3680.

[4] Mayer, Y. D., Lyu, B., Kamliya Jawahar, H., and Azarpeyvand, M., "A Semi-analytical Noise Prediction Model for Airfoils with Serrated trailing-edges", *Renewable Energy*, Vol. 143, 2019, 679-691.

[5] Celik, A., Mayer, Y. D., and Azarpeyvand, M., "An experimental aeroacoustic study on serrated trailing-edge geometries and flow misalignment effects", 26th AIAA/CEAS Aeroacoustics Conference, 2020.

[6] Celik, A., Bowen, L., and Azarpeyvand, M., "Effects of trailing edge bevel angle on the sound generation of a flat plate", 26th AIAA/CEAS Aeroacoustics Conference, 2020.

[7] Celik, A., and Azarpeyvand, M., "Effect of adverse and favorable pressure gradient on hydrodynamic field of a serrated flat plate", 26th AIAA/CEAS Aeroacoustics Conference, 2020.

[8] Showkat Ali, S. A., Azarpeyvand, M., and Ilario, C., "Trailing Edge Flow and Noise Control using Porous Treatments", *Journal of Fluid Mechanics*, Vol. 850, 2018, pp. 83-119.

[9] Showkat Ali, S. A., Szoke, M., Azarpeyvand, M., and Ilario, C., "Turbulent Flow Interaction with Porous Surfaces", AIAA 2018-2801, 2018.

[10] Showkat Ali, S. A., Azarpeyvand, M., Szoke, M. and da Silva, C. R. I., "Boundary layer flow interaction with a permeable wall," *Physics of Fluids*, Vol. 30, 2018, pp. 085111.

[11] Kamliya Jawahar, H., Theunissen, R., Azarpeyvand, M., and Carlos R.Ilario., "Flow characteristics of slat cove fillers", *Aerospace Science and Technology*, Vol. 100, 2020, 105789.

[12] Kamliya Jawahar, H., Showkat Ali, S. A., Azarpeyvand, M., and Ilario, C., "Aerodynamic and aeroacoustic performance of high-lift airfoil fitted with slat cove fillers", *Journal of Sound and Vibration*, Vol. 479, 2020, 115347.

[13] Kamliya Jawahar, H., Showkat Ali, S. A., Azarpeyvand, M., and Carlos R.Ilario., "Aeroacoustic Performance of Three-element High Lift Airfoil with Slat Cove Fillers", AIAA 2019-2440, 2019.

[14] Ai, Q., Kamliya Jawahar, H., and Azarpeyvand, M., "Experimental Investigation of Aerodynamic Performance of Airfoils Fitted with Morphing trailing-edges", AIAA 2016-1563, 2016.

[15] Kamliya Jawahar, H., Azarpeyvand, M., and Silva, C., "Aerodynamic and Aeroacoustic Performance of Airfoils Fitted with Morphing Trailing-edges", AIAA 2018-2815, 2018.

[16] Kamliya Jawahar, H., Ai, Q., and Azarpeyvand, M., "Experimental and Numerical Investigation of Aerodynamic Performance of Airfoils Fitted with Morphing trailing-edges", AIAA 2017-3371, 2017.

[17] Kamliya Jawahar, H., Ai, Q., and Azarpeyvand, M., "Experimental and Numerical Investigation of Aerodynamic Performance of Airfoils with Morphed trailing-edges", *Renewable Energy*, Vol. 127, 2018, pp. 355-367.

[18] Brooks, T. F., and Humphreys, W. M., "Flap-edge aeroacoustic measurements and predictions", *Journal of Sound and Vibration*, Vol. 261, 2003, pp. 31-74.

[19] Howe, M., "On the generation of side-edge flap noise". *Journal of Sound and Vibration*, Vol. 80, 1982, pp. 555-573.

[20] Guo, Y., "On noise reduction by flap side edge fences", *Journal of Sound and Vibration*, Vol. 277, 2004, pp. 369-390.

[21] Angland, D., Zhang, X., and Molin, N., "Measurements of flow around a flap side edge with porous edge treatment", *AIAA Journal*, Vol. 47, 2009, pp. 1660-1671.

[22] Dobrzynski, W., "Almost 40 years of airframe noise research: what did we achieve?". *Journal of Aircraft*, vol. 47, 2010, pp. 353-367.

[23] Hutcheson, F. V., Brooks, T. F., and Humphreys, W. M, "Noise radiation from a continuous mold-line link flap configuration", *International Journal of Aeroacoustics*, Vol. 11, 2012, pp. 565-588.

[24] Pankonien, A. M., Inman, D. J., "Aerodynamic Performance of a Spanwise Morphing trailing-edge Concept", 25th International Conference on Adaptive Structures and Technologies, ICAST2014-004,2014.

[25] Gad-el-Hak, M. *Flow Control: Passive, Active, and Reactive Flow Management*; Cambridge University Press: New York, 2006.

[26] Sanders, B., Eastep, F.F., and Froster, E. "Aerodynamic and Aeroelastic Characteristics of Wings with Conformal Control Surfaces for Morphing Aircraft", *Journal of Aircraft*, Vol. 40, No. 1, pp: 94-99, January 2003.

[27] Daynes, S., and Weaver, M.P., "A Morphing trailing-edge Device for a Wind Turbine", *Journal of Intelligent Material Systems and Structures*, Vol. 23, No. 6, pp: 691-701, March 2012.

[28] Wolff, T., Ernst, B., and Seume, J.R., "Aerodynamic Behaviour of an Airfoil with Morphing trailing-edge for Wind Turbine Application", *The Science of Making Torque from Wind 2014*, June 2014.

[29] Campanile, L.F., and Anders, S., "Aerodynamic and Aeroelastic Amplification in Adaptive Belt-rib Airfoils", *Aerospace Science and Technology*, Vol. 9, pp:55-63, September 2004.

[30] Yokozeki, T., Sugiura,A., and Hirano,Y. "Development of Variable Camber Morphing Airfoil Using Corrugated Structure", *Journal of Aircraft*, Vol. 51, No. 3, pp:1023-1029, May 2014.

[31] Ai, Q., Azarpeyvand, M., Lachenal, X., and Weaver, P., "Aerodynamic and Aeroacoustic Performance of Airfoils Using Morphing Structures", *Wind Energy*, Vol. 19, No. 7, pp:1325-1339, July 2016.

[32] Ai, Q., Azarpeyvand, M., Lachenal, X., and Weaver, P., "Airfoil Noise Reduction Using Morphing trailing-edge", *The 21st International Congress on Sound and Vibration*, Beijing, China., July 2014.

[33] Barrett R.V., "Design and Performance of a New Low Turbulence Wind Tunnel at Bristol University", *The Aeronautical Journal*, Vol. 88, No. 873, pp: 86-90, March 1984.

[34] Lyon, C. A., Selig, M. S., and Broeren, A. P., "Boundary Layer Trips on Airfoils at Low Reynolds Numbers ", AIAA 97-0511 , 1997.

[35] Lyon, C. A., Broeren, A. P., Golalarathnam, A., and Selig, M. S., *Chapter 6: Boundary Layer Trips, Summary of Low-Speed Airfoil Data - Volume 3*, SoarTech Publications: Virginia, 1997, pp:331-341.

[36] Mayer, Y. D., Kamliya Jawahar, H., Szke, M., Ali, S. A. S., and Azarpeyvand, M. "Design and Performance of an Aeroacoustic Wind-tunnel Facility at the University of Bristol", *Applied Acoustics*, Vol. 155, 2019.

[37] Mayer, Y., Zang, B., and Azarpeyvand, M., "Design of a Kevlar-walled Test Section With Dynamic Turntable and Aeroacoustic Investigation of an Oscillating Airfoil", AIAA 2019-2464, 2019.

[38] Devenport, W. J., Burdisso, R. A., Borgoltz, A., Ravetta, P. A., Barone, M. F., Brown, K. A., and Morton, M. A., "The Kevlar-walled anechoic wind tunnel", *Journal of Sound and Vibration*, Vol. 332, 2013, pp: 3971 - 3991.